

first event; and  $E_{F1} = 110$  MeV,  $E_{F2} = 55$  MeV, with  $E_{\text{tot}} = 165$  MeV for the second event.

We searched the recorded data backwards in time from each of those two events for preceding  $\alpha$ -particles correlated in position. For the first case only one  $\alpha$ -particle was detected in the front detector 1.32 s after the implantation in the middle of the strip of a recoil nucleus with a measured energy  $E_{\text{EVR}} = 10$  MeV. This value agrees with the energy expected for the element-114 recoils, and the TOF signal is consistent with that expected for a complete-fusion EVR, as determined in the calibration reactions. The energy of the  $\alpha$ -particle was  $E_{\alpha} = 10.29$  MeV. The SF event was observed 559.6 s later. All the three signals (EVR,  $\alpha$  and SF) appeared within a position interval of 0.82 mm, which indicates that there is correlation between the observed decays. The probability for the observed correlation to be a random coincidence of signals imitating the decay chain (EVR,  $\alpha$  and SF) at a given position window amounts to  $\sim 2 \times 10^{-4}$ . It was calculated employing a method used in the case of low statistics<sup>21</sup>.

In the second case, spontaneous fission was observed 243 s after the registration of the implanted recoil nucleus with the energy  $E_{\text{EVR}} = 13.5$  MeV. In the search for an  $\alpha$ -particle in the time interval EVR–SF, only a single escape signal with  $E_{\alpha 1} = 2.31$  MeV was found 14.45 s after the implantation of the recoil nucleus. All the three signals (EVR,  $\alpha$  and SF) appeared within a position interval of 1.0 mm, which again indicated correlation between the observed decays. The probability for the observed correlation to be a random coincidence of signals of the EVR,  $\alpha$  and SF type in this case is  $3 \times 10^{-3}$ . The entire position-correlated decay chains are shown in Fig. 3a. In both sequences, the parent nucleus undergoes  $\alpha$ -decay. As the total energy  $E_{\alpha}$  for the second event is not determined, we assume that the  $\alpha$ -decay in both the cases proceeds from one and the same state. The decay properties of the parent nucleus are  $T_{\alpha} = 5.5^{+10}_{-2}$  s and  $E_{\alpha} = 10.29 \pm 0.02$  MeV (determined by one event).

In the experiment described here, namely  $^{48}\text{Ca} + ^{242}\text{Pu}$  reaction, 2 neutrons and 2 protons were added to the target in comparison with the previous experiment  $^{48}\text{Ca} + ^{238}\text{U}$ . In this case after the  $\alpha$ -decay (2 neutrons and 2 protons) the EVR of 114 will be transformed to the daughter nucleus with  $Z = 112$ . It is most likely that the  $^{283}112$  daughter nuclei from the reaction  $^{48}\text{Ca} + ^{242}\text{Pu}$  are the same as the nuclei produced directly in the reaction  $^{48}\text{Ca} + ^{238}\text{U}$  (ref. 16) and all of them undergo spontaneous fission. The reason is that the bombarding energy of  $^{48}\text{Ca}$  ions and the corresponding excitation energy of compound nuclei  $^{286}112$  and  $^{290}114$  are very close (in their values) and these compound nuclei could evaporate the same number of neutrons (most probably 3 neutrons). The time intervals measured for all the four spontaneous fission events (this work and ref. 16), as can be seen from Fig. 3a and b, correspond to the same half-life within the limits of the probability errors. It is then possible to conclude that in both the reactions we observe the spontaneous fission of one and the same nuclide with  $T_{\text{SF}} \approx 3$  min. In the  $^{48}\text{Ca} + ^{238}\text{U}$  reaction it was produced directly as an EVR in the 3n-evaporation channel, while in the  $^{48}\text{Ca} + ^{242}\text{Pu}$  reaction it is the daughter from the  $\alpha$ -decay of the parent  $^{287}114$  nucleus. The half-life of the nucleus  $^{283}112$  determined on the basis of the four events amounts to  $T_{\text{SF}} = 180^{+170}_{-60}$  s. From the analysis of the data, we conclude that the observed  $\alpha$ -SF chains arise with a high probability from the decay of the superheavy nucleus, which is the isotope of element 114 with the mass number 287 ( $Q_{\alpha} = 10.44 \pm 0.02$  MeV, where  $Q_{\alpha}$  is the total energy deposited at  $\alpha$ -decay). That nucleus could be produced in the 3n-evaporation channel with the cross-section  $\sigma = 2.5^{+3.3}_{-1.6}$  pb.

The half-life of the new isotope  $^{287}114$  is several times shorter than that of the previously observed heavier isotope  $^{289}114$ , formed in the reaction  $^{48}\text{Ca} + ^{244}\text{Pu}$  (Fig. 3c). Such a trend is expected with a decrease in the neutron numbers of the superheavy nuclei (Fig. 1b).

The observed radioactive properties of the new nucleus  $^{287}114$ , together with the data obtained earlier for the isotope  $^{289}114$  and the products of its  $\alpha$ -decay (namely, the isotopes  $^{283}112$  and  $^{285}112$ ; refs 16, 18) can be considered as experimental proof of the existence of ‘the island of stability’ of superheavy elements. □

Received 19 April; accepted 16 June 1999.

1. Myers, W. D. & Swiatecki, W. J. Nuclear masses and deformations. *Nucl. Phys. A* **81**, 1–60 (1966).
2. Nix, J. R. Calculation of fission barriers for heavy and superheavy nuclei. *Annu. Rev. Nucl. Sci.* **22**, 65–120 (1972).
3. Smolańczuk, R., Skalski, J. & Sobiczewski, A. in *Proc. Int. Workshop XXIV on Gross Properties of Nuclei and Nuclear Excitations “Extremes of Nuclear Structure”* (eds Feldmeier, H., Knoll, J. & Nörenberg, W.) 35–42 (GSI, Darmstadt, 1996).
4. Smolańczuk, R. Properties of the hypothetical spherical superheavy nuclei. *Phys. Rev. C* **56**, 812–824 (1997).
5. Möller, P., Nix, J. R. & Kratz, K.-L. Nuclear properties for astrophysical and radioactive-ion-beam applications. *Atom. Data Nucl. Data Tables* **66**, 131–134 (1997).
6. Oganessian, Yu. Ts. in *Proc. Int. Conf. on Nuclear Physics at the Turn of the Millennium “Structure of Vacuum and Elementary Matter”* (eds Stocker, H., Gallmann, A. & Hamilton, J. H.) 11–24 (World Scientific, Singapore, 1997).
7. Pustylnik, B. I. in *Proc. VI Int. School-Seminar “Heavy Ion Physics”* (eds Oganessian, Yu. Ts. & Kalpakchieva, R.) 431–433 (World Scientific, Singapore, 1998).
8. Wada, T. et al. in *Proc. Int. Conf. on Dynamical Aspects on Nuclear Fission* (eds Oganessian, Yu. Ts. & Kliman, J.) (World Scientific, Singapore, 1999).
9. Gregorich, K. E. et al. First confirmation of the discovery of element 106. *Phys. Rev. Lett.* **72**, 1423–1426 (1994).
10. Schädel, M. et al. Chemical properties of element 106 (seaborgium). *Nature* **388**, 55–57 (1997).
11. Lazarev, Yu. A. et al.  $\alpha$  decay of  $^{273}110$ : shell closure at  $N = 162$ . *Phys. Rev. C* **54**, 620–625 (1996).
12. Blocki, J. P., Feldmeier, H. & Swiatecki, W. J. Dynamical hindrance to compound-nucleus formation in heavy-ion reactions. *Nucl. Phys. A* **459**, 145–172 (1986).
13. Hulet, E. K. et al. Search for superheavy elements in the bombardment of  $^{248}\text{Cm}$  with  $^{48}\text{Ca}$ . *Phys. Rev. Lett.* **39**, 385–389 (1977).
14. Oganessian, Yu. Ts. et al. Experiments to produce isotopes of superheavy elements with atomic numbers 114–116 in  $^{48}\text{Ca}$  ion reactions. *Nucl. Phys. A* **294**, 213–224 (1978).
15. Armbruster, P. et al. Attempts to produce superheavy elements by fusion of  $^{48}\text{Ca}$  with  $^{248}\text{Cm}$  in the bombarding energy range of 4.5–5.2 MeV/u. *Phys. Rev. Lett.* **54**, 406–409 (1985).
16. Oganessian, Yu. Ts. et al. Search for new isotopes of element 112 by irradiation of  $^{238}\text{U}$  with  $^{48}\text{Ca}$ . *Eur. Phys. J. A* **5**, 63–68 (1999).
17. Hofmann, S. et al. The new element 112. *Z. Phys. A* **354**, 229–230 (1996).
18. Oganessian, Yu. Ts. et al. The synthesis of superheavy nuclei in the  $^{48}\text{Ca} + ^{244}\text{Pu}$  reaction. *Phys. Rev. Lett.* (submitted); also as preprint E7-99-53 (JINR, Dubna, 1999).
19. Kutner, V. B. et al. in *Proc. 15th Int. Conf. on Cyclotrons and Their Applications* (eds Baron, E. & Lieuvain, M.) 405–408 (IOP, Bristol, 1998).
20. Yereimin, A. V. et al. The kinematic separator VASSILISSA performance and experimental results. *Nucl. Instrum. Meth. A* **350**, 608–617 (1994).
21. Schmidt, K.-H. et al. Some remarks on the error analysis in the case of poor statistics. *Z. Phys. A* **316**, 19–26 (1984).

**Acknowledgements.** We thank the JINR Directorate, in particular Ts. Vylou, V. G. Kadyshesky and A. N. Sissakian, for help and support; V. Ya. Lebedev and S. N. Dmitriev for the preparation of metal Ca samples for the ECR-ion source; A. N. Shamanin and E. N. Vornokov for help in the maintenance of the recoil separator; G. Münzenberg, A. Sobiczewski and R. Smolańczuk for discussions; the staff of the U-400 Cyclotron for assistance; and V. N. Loginov, A. N. Lebedev, and the ion source group staff for obtaining the intense  $^{48}\text{Ca}$  beam. This work was supported by the Russian Foundation for Basic Research and the INTAS, largely through the Russian Ministry of Atomic Energy.

Correspondence and requests for materials should be addressed to A.V.Y. (e-mail: ereimin@sunvas.jinr.ru).

## Observation of negative electron-binding energy in a molecule

Xue-Bin Wang & Lai-Sheng Wang

Department of Physics, Washington State University, Richland, Washington 99352, USA and W. R. Wiley Environmental Molecular Sciences Laboratory, Pacific Northwest National Laboratory, MS K8-88, PO Box 999, Richland, Washington 99352, USA

In neutral atoms and molecules, electrons are kept within their orbitals by attractive electrostatic interactions with positively charged nuclei, with relatively few neutral molecules being able to bind more than one extra electron. For multiply charged molecular anions, dynamic stability plays an important role: the superposition of long-range Coulomb repulsion and short-range electron binding gives rise to a repulsive Coulomb barrier (RCB) that traps the excess electrons<sup>1</sup>. The RCB has profound effects on the physical and chemical properties of multiply charged anions

in the gas phase<sup>1–5</sup>. For example, it has recently been shown to prevent the detachment of electrons from a doubly charged anion, even when the excitation energies exceed the electron binding energy<sup>6,7</sup>. Here we report photodetachment experiments which demonstrate that the RCB can even trap electrons in molecular orbitals characterized by a negative binding energy. We show that the addition of sulphate groups ( $-\text{SO}_3^-$ ) to cyclic copper phthalocyanine (CuPc; ref. 8) systematically increases the energy of the corresponding molecular orbitals, culminating in the highest occupied molecular orbital of the tetra-anion,  $[\text{CuPc}(\text{SO}_3)_4]^{4-}$ , being unstable by 0.9 eV. The increase in molecular orbital energy and the negative electron binding energy we observe are due to charge localization in the sulphate groups and the resultant RCB. The unusually large height of the repulsive barrier also ensures that the anion remains metastable, and continues to store 0.9 eV excess electrostatic energy, throughout the 400 seconds we are able to observe it.

Details of the experimental apparatus have been given elsewhere<sup>9</sup>. Our experiment involves generation of gas-phase multiply charged negative ions using electrospray and photodetachment photoelectron spectroscopy (PES) of size- and charge-selected anions. The electrospray solution is a  $10^{-4}$  M CuPc-3, 4', 4'', 4'''-tetrasulphonate sodium salt solution in a water/methanol (2/98 ratio) mixed solvent at neutral pH. The anions produced from the electrospray are accumulated and stored in a quadrupole ion trap for 0.1 s at a pressure of  $10^{-4}$  torr before being analysed by a time-of-flight mass spectrometer. We use two detachment photon energies ( $h\nu$ ), 6.424 eV (193 nm wavelength) and 4.661 eV (266 nm), and measure the kinetic energies (KE) of the photoemitted electrons using a magnetic-bottle time-of-flight electron analyser. The measured distributions of electron times of flight are converted to KE spectra calibrated using the known spectra of  $\text{I}^-$  and  $\text{O}^-$ . The electron binding energies (BE) are determined from Einstein's photoelectric equation,  $h\nu = \text{BE} + \text{KE}$ .

Figure 1a and b shows the spectra of  $[\text{CuPc}(\text{SO}_3)_4]^{4-}$  tetra-anions at the two detachment energies. The 193-nm spectrum reveals a weak feature (X) at negative binding energies with a threshold energy of  $-0.9$  eV and two broad features (A and B) at positive binding energies. The observation of the negative-binding-energy feature is remarkable, indicating that the tetra-anion is unstable with respect to an electron loss. The photoelectron KE corresponding to the negative-binding-energy feature is 7.32 eV at 193 nm, that

is, 0.9 eV higher than the photon energy. The electron energy scales are carefully calibrated and the surprising observation of the negative electron binding energy is reproducible (see also Fig. 1 legend). At 266 nm, the negative-binding-energy feature becomes dominant; the higher-binding-energy feature B disappears and only a tail of feature A is observed. Figure 1c and d shows the spectra of the triply charged monoprotanated species,  $[\text{CuPc}(\text{SO}_3)_4\text{H}]^{3-}$ , at 266 and 193 nm. The features of the 193-nm spectrum of the trianion (Fig. 1d) is similar to that of the tetra-anion (Fig. 1b) except that the trianion spectrum is shifted to higher binding energies with a threshold energy at 1.2 eV. Again at 266 nm, the higher-binding-energy features of the trianion spectrum disappear (Fig. 1c). The photon-energy dependence of the PES features of both the tetra- and trianions are consistent with the existence of the RCB and the multiply charged nature of these species<sup>6,7</sup>.

We note that the PES spectra of Fig. 1b and d are rather similar to that of the neutral parent CuPc molecule in the vapour phase except that neutral CuPc has a much higher BE with a threshold ionization potential of 6.3 eV (ref. 10). The similarity between the PES spectra of the present charged species and that of the parent CuPc suggests that detachment occurs from molecular orbitals of mainly CuPc character in the tetra- and trianions. This can be understood from the localized nature of the  $-\text{SO}_3^-$  groups and the electrostatic interactions within the charged species. Our PES spectra of the benzene-sulphonate anion ( $\text{C}_6\text{H}_5-\text{SO}_3^-$ ) and other singly charged sulphonate species show two detachment features from the  $-\text{SO}_3^-$  group separated by 0.6 eV with a threshold binding energy of  $\sim 5$  eV (X.-B.W. and L.-S.W., unpublished results). In the tetra-anion, the electron binding energy in  $-\text{SO}_3^-$  is expected to be reduced owing to the Coulomb repulsion from the other three negative charges. Figure 2 shows a schematic molecular structure of the tetra-anion and the estimated distances between the charge centres and between the central Cu atom and the charge centres<sup>11</sup>. The  $-\text{SO}_3^-$  group at position 1 experiences the largest Coulomb repulsion, which amounts to  $\sim 3.8$  eV ( $\sum_{n=2}^4 e^2/R_{1n}$ ). Therefore, electrons on this  $-\text{SO}_3^-$  group are still expected to be bound by at least 1.2 eV ( $5 - 3.8$  eV). However, the four negative charges create a 7.2 eV ( $\sum_{n=1}^4 e^2/R_{ns}$ ) negative potential on the central Cu atom; that is, an electron localized on Cu would experience a Coulomb repulsion of 7.2 eV. Previous density functional calculations predict that the highest occupied molecular orbital (HOMO) of CuPc is a Cu  $d_\pi$  orbital with a single occupancy ( $11b_{2g}$ , Fig. 3a)<sup>12</sup>.

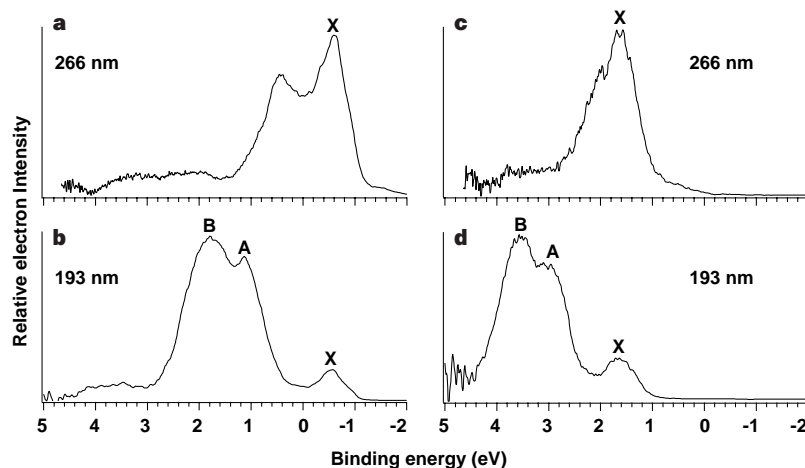


**Figure 1** Photodetachment spectra of  $[\text{CuPc}(\text{SO}_3)_4]^{4-}$  and  $[\text{CuPc}(\text{SO}_3)_4\text{H}]^{3-}$  at 266 and 193 nm. **a** and **b**,  $[\text{CuPc}(\text{SO}_3)_4]^{4-}$ ; **c** and **d**,  $[\text{CuPc}(\text{SO}_3)_4\text{H}]^{3-}$ . Note the negative electron-binding-energy feature (X) of the tetra-anion and the rigid shift to higher binding energies of the trianion spectra. The energy scale is calibrated before and after each experiment to ensure accurate measurements of electron kinetic energies. The energy shifts are typically  $<10$  meV within a 14-h experiment. The spectra are measured several times a month and are highly reproducible, being

independent of source conditions (temperature and pressure). Multiphoton processes are ruled out because the same negative-binding-energy feature is observed with different photon fluxes and at various detachment laser wavelengths. Population of an excited state of the tetra-anion may give a negative electron-binding energy, but is unlikely owing to the multiple-collision conditions of the ion source and ion-trap, and the relatively long timescale of the experiments.

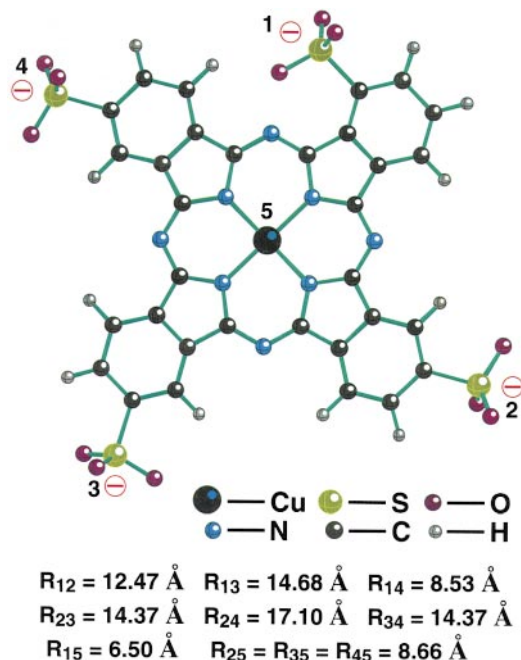


**Figure 2** Structure of the  $[\text{CuPc}(\text{SO}_3)_4]^{4-}$  tetra-anion as determined in bulk crystals (ref. 11). The location of the charges, and the distances between the charge centres and between the charge centres and the central Cu atom are shown. Our optimization with the Spartan software package gives similar structural parameters<sup>13,14</sup>.

A nitrogen  $p_\pi$  orbital ( $2a_{1u}$ , Fig. 3a) is close to the HOMO. As schematically shown in Fig. 3c, the HOMO of the CuPc will be shifted up by 7.2 eV, due to the Coulomb repulsion from the four negative charges on the peripheral  $-\text{SO}_3^-$ , giving rise to a  $-0.9$  eV ( $6.3 - 7.2$  eV) binding energy. This estimated binding energy is in agreement with the experimental observation, despite the qualitative nature of the procedure. In the trianion, the most likely protonation position is on the  $-\text{SO}_3^-$  group at position 1 (Figs 2 and 3b). The Coulomb repulsion at the central Cu due to the three charges (at positions 2, 3, and 4) is now reduced to 5 eV ( $\sum_{n=2}^4 e^2/R_{n5}$ ), again in agreement with the experimental observation that the trianion has a positive binding energy of 1.2 eV. Therefore, we are seeing a stepwise change of the HOMO of CuPc due to the charging at its periphery. Semiempirical calculations using the SPARTAN software package<sup>13</sup> (which uses the PM3 and PM3TM hamiltonians<sup>14</sup>) show that indeed there is a stepwise rigid shift of the molecular orbitals of CuPc due to the negative charges and predicts a negative binding energy for the HOMO of the tetra-anion (K. Ferris, X.-B.W. & L.-S.W., manuscript in preparation). The calculations further confirm that there is little mixing between the molecular orbitals of  $-\text{SO}_3^-$  and those of CuPc, and that the charges are indeed localized on the  $-\text{SO}_3^-$  groups.

Electrons are always bound in a neutral atom or molecule by the Coulomb force due to the positive core. Relatively few neutral molecules can bind more than one extra electron. A negative electron-binding energy has, to our knowledge, not been observed before, because it cannot exist in neutral or singly charged species. It can only happen in multiply charged anions due to the strong Coulomb repulsion among the excess negative charges. Unlike photoionization of a neutral species (or singly charged anion) where the outgoing electron always experiences a long-range attractive force (Fig. 3a), photoemitted electrons from multiply charged anions experience a long-range Coulomb repulsive force. The short-range electron binding and the long-range Coulomb repulsion create a potential barrier against electron loss in multiply charged anions<sup>1-3,5</sup> (Fig. 3b and c). Therefore, even when a photon energy is higher than the electron binding energies in a multiply charged

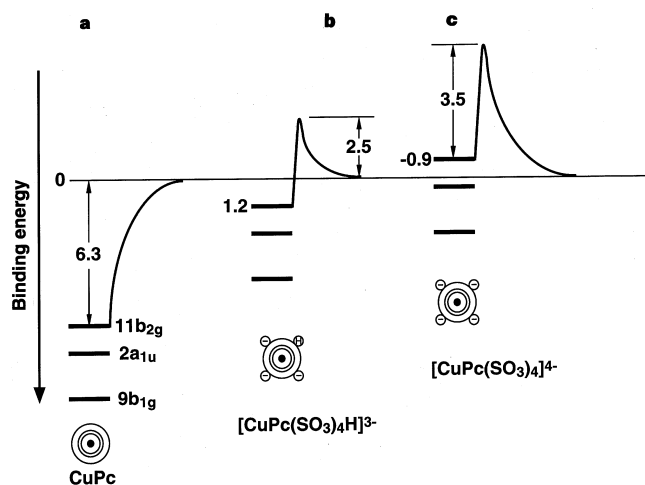


**Figure 3** Schematic diagrams showing the top three molecular orbitals of the parent CuPc molecule and the rigid upshift of these orbitals due to the addition of three and four negative charges. **a**, Parent CuPc; **b**,  $[\text{CuPc}(\text{SO}_3)_4\text{H}]^{3-}$ ; **c**,  $[\text{CuPc}(\text{SO}_3)_4]^{4-}$ . The 'cartoons' show the cyclic neutral CuPc molecule and the sequential charging at its periphery. Schematic potential-energy curves for removing an electron from the highest occupied orbital of the respective species are shown, illustrating the long-range attraction in the CuPc case (**a**), and both the Coulomb barrier and the negative electron-binding energy in the tetra-anion. The experimentally determined electron-binding energies and the Coulomb barrier heights (in eV) are indicated. The 6.3-eV ionization potential of CuPc is from ref. 10.

anion, photoelectrons may not be observed due to the RCB<sup>6,7</sup>, as demonstrated in the 266-nm spectra of the tri- and tetra-anion (Fig. 1). We estimate that the tri- and tetra-anion possess a barrier height of 2.5 and 3.5 eV, respectively, as shown in Fig. 3. The tetra-anion with a negative electron-binding energy is metastable, and in fact stores 0.9 eV excess electrostatic energy. We can estimate the lifetime of this metastable anion with our ion-trap<sup>9</sup>. We observe no measurable ion loss within the 400 s that we can store the ions. The long lifetime of this metastable tetra-anion in the gas phase is attributed to the large barrier height and the large size of the molecule; the latter means that the electron has to tunnel a long distance to escape. The repulsive Coulomb barrier can be viewed as an electrostatic 'corral' in this semiplanar molecule, trapping the negatively bound electrons inside. These anions can thus be viewed as an electrostatic energy storage medium in the gas phase or a 'molecular capacitor'. They can also be considered as a molecular analogue of a bulk charged metal surface, where the workfunction combined with the electric field around the metal surface creates a potential barrier (the Schottky effect)<sup>15</sup>, similar to that shown in Fig. 3c. The RCB in multiply charged anions is analogous to the Coulomb barrier experienced in the  $\alpha$ -decay of radioactive nuclei (see, for example, ref. 16). Similar Coulomb barriers against molecular fragmentation exist in multiply charged molecular ions (both anions<sup>17-19</sup> and cations<sup>20-22</sup>), and provide dynamic stability to such species. □

Received 4 February; accepted 1 June 1999.

- Scheller, M. K., Compton, R. N. & Cederbaum, L. S. Gas-phase multiply charged anions. *Science* **270**, 1160-1166 (1995).
- Jin, C. *et al.* Attachment of two electrons to  $\text{C}_{60}\text{F}_{48}$ : Coulomb barrier in doubly charged anions. *Phys. Rev. Lett.* **73**, 2821-2824 (1994).
- Compton, R. N., Tuinman, A. A., Klots, C. E., Peterson, M. R. & Patton, D. C. Electron attachment to a negative ion:  $e + \text{C}_{84}^- \rightarrow \text{C}_{84}^{2-}$ . *Phys. Rev. Lett.* **78**, 4367-4370 (1997).
- Martin, R. L. & Ritchie, J. P. Coulomb and exchange interactions in  $\text{C}_{60}^-$ . *Phys. Rev. B* **48**, 4845-4849 (1993).
- Yannouleas, C. & Landman, U. Stabilized-jellium description of neutral and multiply charged fullerenes  $\text{C}_{60}^{\pm}$ . *Chem. Phys. Lett.* **217**, 175-185 (1994).
- Wang, X. B., Ding, C. F. & Wang, L. S. Photodetachment spectroscopy of a doubly charged anion: direct observation of the repulsive Coulomb barrier. *Phys. Rev. Lett.* **81**, 3351-3354 (1998).
- Wang, L. S., Ding, C. F., Wang, X. B. & Nicholas, J. B. Probing the potential barriers and intramolecular electrostatic interactions in free doubly charged anions. *Phys. Rev. Lett.* **81**, 2667-2670 (1998).

8. Leznoff, C. C. & Lever, A. B. P. (eds) *Phthalocyanines: Properties and Applications* (VCH, New York, 1989).
9. Wang, L. S., Ding, C. F., Wang, X. B. & Barlow, S. E. Photodetachment photoelectron spectroscopy of multiply charged anions using electrospray ionization. *Rev. Sci. Instrum.* **70**, 1957–1966 (1999).
10. Berkowitz, J. Photoelectron spectroscopy of phthalocyanine vapors. *J. Chem. Phys.* **70**, 2819–2828 (1979).
11. Brown, C. J. Crystal structure of  $\beta$ -copper phthalocyanine. *J. Chem. Soc. A* 2488–2493 (1968).
12. Rosa, A. & Baerends, E. J. Metal-macrocycle interaction in phthalocyanines: density functional calculations of ground and excited states. *Inorg. Chem.* **33**, 584–595 (1994).
13. PC Spartan Plus 5.1 (Wavefunction, Inc., Von Carman Ave., Irvine, California 92612, USA).
14. Stewart, J. J. Optimization of parameters for semiempirical methods II: Applications. *J. Comput. Chem.* **10**, 221–264 (1989); MOPAC: A semiempirical molecular orbital program. *J. Comput. Aided Mol. Design* **4**, 1–105 (1990).
15. D'Haennens, I. J. in *Encyclopedia of Physics* (eds Lerner, R. G. & Trigg, G. L.) 1251–1253 (VCH, New York, 1991).
16. Hodgson, P. E., Gadioli, E. & Erba, E. G. *Introductory Nuclear Physics* (Clarendon, Oxford, 1997).
17. Scheller, M. K. & Cederbaum, L. S. A construction principle for stable multiply charged molecular anions in the gas phase. *Chem. Phys. Lett.* **216**, 141–146 (1993).
18. Weikert, H.-G. & Cederbaum, L. S. Free doubly negative tetrahalides. *J. Chem. Phys.* **99**, 8877–8891 (1993).
19. Boldyrev, A. I., Gutowski, M. & Simons, J. Small multiply charged anions as building blocks in chemistry. *Acc. Chem. Res.* **29**, 497–502 (1996).
20. Vekey, K. Multiply charged ions. *Mass Spectrom. Rev.* **14**, 195–225 (1995).
21. Brechignac, C., Cahuzac, P., Kebaili, N. & Leygnier, J. Temperature effects in the Coulombic fission of strontium clusters. *Phys. Rev. Lett.* **81**, 4612–4615 (1998).
22. Schroder, D., Harvey, J. N. & Schwarz, H. Long-lived, multiply charged diatomic  $\text{TiF}^{n-}$  ions ( $n = 1-3$ ). *J. Phys. Chem. A* **102**, 3639–3642 (1998).

**Acknowledgements.** We thank R. S. Disselkamp for discussions and K. Ferris for help in the theoretical calculations. This work was supported by the US Department of Energy, Office of Basic Energy Sciences, Chemical Sciences Division and is conducted at the Pacific Northwest National Laboratory, operated for the US Department of Energy by Battelle Memorial Institute. L.-S.W. is an Alfred P. Sloan research fellow.

Correspondence and requests for materials should be addressed to L.-S.W. (e-mail: ls.wang@pnl.gov).

## Dual modes of the carbon cycle since the Last Glacial Maximum

H. Jesse Smith\*, H. Fischer\*†, M. Wahlen\*, D. Mastroianni\* & B. Deck\*

\* Scripps Institution of Oceanography, University of California San Diego, La Jolla, California 92093-0220, USA

The most conspicuous feature of the record of past climate contained in polar ice is the rapid warming which occurs after long intervals of gradual cooling. During the last four transitions from glacial to interglacial conditions, over which such abrupt warmings occur, ice records indicate that the  $\text{CO}_2$  concentration of the atmosphere increased by roughly 80 to 100 parts per million by volume (refs 1–4). But the causes of the atmospheric  $\text{CO}_2$  concentration increases are unclear. Here we present the stable-carbon-isotope composition ( $\delta^{13}\text{C}$ ) of  $\text{CO}_2$  extracted from air trapped in ice at Taylor Dome, Antarctica, from the Last Glacial Maximum to the onset of Holocene times. The global carbon cycle is shown to have operated in two distinct primary modes on the timescale of thousands of years, one when climate was changing relatively slowly and another when warming was rapid, each with a characteristic average stable-carbon-isotope composition of the net  $\text{CO}_2$  exchanged by the atmosphere with the land and oceans.  $\delta^{13}\text{C}$  increased between 16.5 and 9 thousand years ago by slightly more than would be estimated to be caused by the physical effects of a  $5^\circ\text{C}$  rise in global average sea surface temperature driving a  $\text{CO}_2$  efflux from the ocean, but our data do not allow specific causes to be constrained.

Carbon dioxide in the atmosphere causes a radiative forcing second only to water vapour, and so may be a central agent in climate change. Polar ice cores contain a detailed record of climate-

related variables which extends more than 400,000 years into the past<sup>4</sup>, and are especially valuable for studying variations of atmospheric  $\text{CO}_2$  as they contain an effectively direct record, unlike atmospheric proxies such as marine carbonates or preserved organic material<sup>5</sup> which may also reflect biological effects. Ice cores from Antarctica, such as those of Taylor Dome and Vostok, are the best sources for palaeoatmospheric  $\text{CO}_2$  measurements because they contain only small amounts of the kinds of chemical impurities, such as carbonate dust or organic acids, that may lead to contamination by *in situ*  $\text{CO}_2$  production<sup>2,6–8</sup>. Taylor Dome ice has the additional advantage that the entire 554-m-long core is from above the depth at which air trapped in bubbles in the ice forms gas-ice clathrates. This feature is important because, as we have found, the accuracy of  $\delta^{13}\text{C}$  measurements performed on bubble-free ice may be affected by the presence of clathrates. ( $\delta^{13}\text{C}$  is defined in Methods.) We have measured the  $\text{CO}_2$  concentration and  $\delta^{13}\text{C}$  of air trapped in ice from Taylor Dome, Antarctica, across the last glacial termination in order to develop a time series for the carbon-isotope composition of atmospheric  $\text{CO}_2$  and to constrain the mechanisms of carbon cycling between the main sources and sinks of atmospheric  $\text{CO}_2$ .

The atmospheric  $\text{CO}_2$  concentration data<sup>3,9</sup> (Fig. 1) form a record comparable to that from Byrd and Vostok<sup>1,2</sup>. The salient features include a low but variable concentration of atmospheric  $\text{CO}_2$  between 27.1 and 18.0 kyr BP (thousand years before present, where “present” is defined as AD 1950), when it varied between 186 and 201 parts per million by volume (p.p.m.v.); a rise, at a fairly constant rate, from 190 p.p.m.v. at 17.0 kyr BP to an early Holocene local maximum of 268 p.p.m.v. at 10.6 kyr BP, punctuated by a shallow minimum at 16.1 kyr BP and a drop of 8 p.p.m.v. between 14 and 13 kyr BP which may be related to the Antarctic Cold Reversal<sup>3</sup>; an 8 p.p.m.v. decrease, from 268 p.p.m.v. at 10.6 kyr BP to 260 p.p.m.v. at 9.1 kyr BP, followed by a rise to the pre-industrial level of about 280 p.p.m.v. (as discussed in detail by Indermühle *et al.*<sup>9</sup>). These data can be combined with the carbon-isotope composition of the  $\text{CO}_2$  to give a better picture of how the carbon cycle operated during this time.

The main features of the carbon-isotope record shown in Fig. 1 include a 0.5‰ drop in  $\delta^{13}\text{C}$  between 18.0 and 16.5 kyr BP, and the subsequent increase of 0.7‰, from  $-7.0\text{‰}$  to  $-6.3\text{‰}$ , between 16.5 and 9.1 kyr BP, which is interrupted by two local  $\delta^{13}\text{C}$  minima at approximately 13 and 10 kyr BP. The minimum-to-maximum  $\delta^{13}\text{C}$  increase began 1,000 to 2,000 years after  $\text{CO}_2$  began to rise, and continued to rise for  $\sim 3,000$  years after the  $\text{CO}_2$  concentration maximum at 10.6 kyr BP, which we interpret as a consequence of the bimodality of carbon cycling (discussed below) rather than a decoupling of  $\text{CO}_2$  concentrations from carbon-isotope compositions. Furthermore, there appears to have been an extended local minimum in  $\delta^{13}\text{C}$  between 13.4 and 12.3 kyr BP that accompanied the Younger Dryas<sup>10</sup> but was not concurrent with the  $\text{CO}_2$  concentration drop at 14 kyr BP. The 0.16‰ difference between the average  $\delta^{13}\text{C}$  values of the Last Glacial Maximum (LGM) and Holocene (see Fig. 2 legend for an explanation of these groupings) is similar to the increase of  $0.19 \pm 0.18\text{‰}$  estimated by Leuenberger *et al.*<sup>11</sup> to have occurred between the period 20–40 kyr BP and the early Holocene. These data show, however, that there was a significant drop in  $\delta^{13}\text{C}$  between the end of the LGM and the beginning of the transition, and that the subsequent rise into the early Holocene was much larger than the difference between average values for the LGM and Holocene. Moreover, inferences about the carbon cycle drawn from the comparison of the LGM and Holocene averages may be misleading because there was significant variability within each of those periods, and the averages depend strongly on the interval chosen to calculate them. Finally, the variability of  $\delta^{13}\text{C}$  before 17.5 kyr BP and after 10.3 kyr BP, 0.33‰ and 0.37‰, respectively, is about half of the magnitude of the

† Present address: Alfred-Wegener-Institute for Polar and Marine Research, Columbusstrasse, D-27515 Bremerhaven, Germany.